Proceedings of ASME Turbo Expo 2024
Turbomachinery Technical Conference and Exposition
GT2024
June 24-28, 2024, London, United Kingdom

GT2024-124983

1D MODELLING OF A WATER-STEAM EJECTOR AS A COMPRESSION STEP IN HIGH-TEMPERATURE HEAT PUMPS

Omar Abu Khass[1,*], A. Phong Tran[1], Steffen Klöppel[1], Panagiotis Stathopoulos [1], Eberhard Nicke [1]

[1]German Aerospace Center, Institute of Low-Carbon Industrial Processes, Cottbus/Zittau, Germany

ABSTRACT

High-temperature heat pumps (HTHPs) have emerged as a promising solution for decarbonizing process heat. With natural refrigerants like water, Rankine cycle-based HTHPs can deliver process heat up to 200°C, which covers a wide range of industrial processes. However, achieving these high temperatures necessitates advanced turbomachinery. Current designs processes for steam compressors are intricate and often tailored for specific applications. Furthermore, achieving the desired temperature typically requires multiple compressors, adding to the complexity of the system. To address this, ejectors can be utilized as a secondary steam compression mechanism within the heat pump architecture. By integrating an ejector, a portion of the heat pump condensate can be used and mixed with superheated steam from the compressor to simultaneously de-superheat the steam and raise its pressure. This approach can potentially reduce both compression power and the number of compression stages required. This paper presents a one-dimensional mathematical model of a water-steam two-phase ejector designed for HTHPs. Using thermodynamic 1D modelling, differential conservation equations and the IAPWS-IF97 equations of state are applied across the ejector's components, accounting for flow compressibility and its two-phase nature. Closing equations are used in the mixing and diffuser sections to simulate the transfer of mass, momentum, and energy between the two streams, assuming homogeneous equilibrium. A specific use case for the ejector's integration in a high-temperature heat pump cycle identified the boundary conditions for the simulations. The model enables the calculation of the 1D distribution of flow variables and key ejector performance indicators, such as the pressure ratio. This research offers advancements in two-phase water steam ejector modelling, shedding light on their potential as steam compression devices in HTHPs.

Keywords: Two-phase ejector, Mathematical modelling, Rankine cycle heat pump, Steam compression

*Corresponding author: omar.abukhass@dlr.de

NOMENCLATURE

Roman letters

A	area [m^2]
c	speed of sound [$m\ s^1$]
D	Diameter [m]
F	Lateral surface area [m^2]
k	thermal conductivity [$W\ m^{-1}\ K^{-1}$]
h	specific enthalpy [$J\ kg^{-1}$]
m	mass [kg]
p	pressure [Pa]
Re	Reynolds number
s	specific entropy [$J\ kg^{-1}\ K^{-1}$]
T	temperature [K]
v	specific volume [$m\ kg^{-3}$]
W	force [$kg\ m\ s^{-2}$]
w	Velocity [$m\ s^{-1}$]
x	axial coordinate [m]

Greek letters

α	heat transfer coefficient [$W\ m^{-2}\ K^{-1}$]
β	void fraction [-]
χ	vapor mass fraction [-]
ϵ	absolute roughness [m]
κ	isentropic expansion coefficient [-]
Γ	mass transfer rate [$kg\ s^{-1}$]
η	dynamic viscosity [$kg\ m^{-1}\ s^{-1}$]
Π	momentum transfer rate [$kg\ m\ s^{-2}$]
ρ	Density [$kg\ m^{-3}$]
ζ	nozzle efficiency [-]

Dimensionless groups

a	coefficient of scale
B	array of source terms
C	drag coefficient
f	friction factor
M	Mach number
$\boldsymbol{X}$	array of state variables
$\boldsymbol{\Omega}$	coefficients matrix

Superscripts and subscripts

as	after shock
bs	before shock
e	evaporation
f	friction
h	hydraulic diameter
int	interface
l	saturated liquid
m	motive stream
mn	motive nozzle
mix	mixer
n	nozzle
s	suction stream
sat	saturation
sn	suction nozzle
T	transpose matrix
v	saturated vapor
∞	local equilibrium

Abbreviations

COP	coefficient of performance
$HTHP$	high-temperature heat pump

1. INTRODUCTION

High-temperature heat pumps (HTHPs) have emerged as a vital solution in the energy transition towards carbon-free heating processes, particularly when powered by renewable electricity. As highly attractive energy conversion devices, they offer efficient means to reduce primary energy consumption in industrial processes through waste heat recovery [1]. Among various working fluids, water is increasingly recognized for its environmental friendliness, exhibiting high latent heat and a critical temperature of 374°C, ideal for HTHP applications. This recognition has increased the research on water HTHPs, aiming to optimize their efficiency and integration into modern energy systems [2, 3]. Despite these advantages, the implementation of water HTHPs faces significant technical challenges, primarily in the development of efficient steam compressors. The low density of the water vapor phase and its steep boiling curve necessitate multiple compressor stages with intermediate cooling [1]. This complexity not only intensifies design and operational costs but also hinders the market adoption of HTHPs. Consequently, there is an increasing need to study and implement efficient water compression technologies and investigate alternative steam compression solutions. Ejectors driven by high pressure condensate allow to de-superheat the steam from the compressor outlet, while simultaneously increasing its pressure. Thereby, the required power for compression as well as the number of compression stages can be reduced for a given temperature lift.

Ejectors are passive devices that are commonly integrated in refrigeration systems due to the lack of moving parts, limited maintenance and low investment cost [4]. In an ejector, two fluids are mixed; a high-pressure motive fluid is accelerated in a nozzle creating an expansion zone. This zone entrains a suction fluid of low pressure. The two fluids mix in the ejector body where mass, momentum and energy are exchanged between the two. This mixing process results in an increase of the suction fluid pressure which is referred to as pressure lift [5]. The exact nature of the interactions between the two-fluids depend on the cycle within which the ejector is integrated. Two-phase ejectors have been extensively investigated and studied both numerically and experimentally in CO_2 cycles. This field of research is very rich of publications concerning zero-dimensional (0D), one-dimensional (1D) and computational fluid dynamics (CFD) simulations that have been in continuous development and validation against experimental results in the last three decades. An experimental work conducted on the use of two-phase ejectors in a transcritical CO_2 vapor jet refrigeration cycle has been done by Elbel and Hrnjak [6]. Their work revealed that the efficiency of the ejector-equipped CO_2 heat pump system could increase by about 10 % in comparison to a system without an ejector. On the other side, compared to the well-researched CO_2 ejectors, research on two-phase water ejectors is relatively scarce, leaving a gap in the field.

Šarevski and Šarevski [7, 8] have made theoretical and experimental contributions to two-phase water ejectors through investigations in this field, which are documented in several publications. Their work encompasses an assessment of water ejector performance and extends to provide guidelines on design optimizations. Furthermore, they have provided optimized geometrical ratios for ejector components, a factor that is crucial in defining the working mode and ultimately the efficiency of the device [9]. However, the operating parameters for the water-ejectors investigated by Šarevski and Šarevski are different than those under which water ejectors will be operated in HTHPs. Moreover, the vast majority of existing numerical studies on two-phase ejector's are based on 0D or pseudo 1D models, which, while practical, offer only a general estimations of ejector performance. The Munday and Bagster [10] model, which has been later improved by Huang et al. [11] is one of the most known and used 0D models for ejectors. With careful calibration and physics based assumptions of the efficiencies for the different parts of the ejector, a good agreement with experimental results can be achieved by this model [5]. However, the capabilities of this type of modelling for two-phase ejectors is very limited.

Ejectors encompass a vast range of physical phenomena. Although the motive and suction fluids are often single-phase upon entering the ejector, phase changes are common in the ejector body [12]. Additionally, interaction of the two-fluids can result in the formation of shocks downstream of the ejector body [9]. Factors such as velocity difference and temperature difference between the two-mixing streams significantly affect the ejector performance. 1D models are an improved version of simulations and provide a better understanding of the interactions happening in the ejector especially when dealing with two-phase flow. Different zones in the ejector can be represented by suitable equations for mass-, momentum and energy balances combined with a suitable equation of state and closure relations. Banasiak and Hafner [13] developed a one-dimensional, spatially distributed steady-state CO_2 ejector model, demonstrating excellent alignment with experimental results. This modelling approach offers significant insights into the design and efficiency of ejectors. However, its main limitation lies in the fluid-specific parameters of the correlations used to describe the momentum exchange between motive and suction streams. Recently, the model was furthered enhanced and developed by Wilhelmsen et al. [12].

The ejector type studied in this paper is an unconventional way of how ejectors are normally operated. Two-phase CO_2 ejectors are mostly used before the compressor in a heat pump cycle as an expansion energy recovery device and to increase the pressure before the compressor's inlet. On the other hand, the aim of the ejector investigated here is slightly different. Here, highly superheated steam coming from the compressor is intended to be mixed with pressurized condensate in an attempt to further increase the final pressure in the cycle and de-superheat the steam. Such a concept has been first presented by Bergander [14] and has been followed by a study lately done by Alam and Elbel [15]. Both studies have highlighted the potentials of using the ejector in such configuration. For example, Bergander [14] have reported an increase of almost 10% in the heat pump coefficient of performance (COP) by using such an ejector. However, none of the studies have considered the use of water as a working fluid.

The present research investigates the two-phase dynamic flow interaction between water and steam in an ejector for HTHPs application. Preliminary 0D modelling efforts have been done to analyse the boundary conditions that govern the operational feasibility of the ejector [16]. Building on this foundational work, the investigation will progress towards a detailed exploration of the ejector dynamics through a 1D modelling approach, aiming to further understand the underlying physical phenomena governing the system. In this paper the 1D modelling developed by Wilhelmsen et al. [12] and Banasiak and Hafner [13] has been adapted for simulating two-phase water-steam ejector for HTHPs applications. The focus of the simulations is based on the ejector mixer. Continuity, momentum and energy equations were solved at each spatial distribution along the ejector's mixer. The equations are combined with closure relations representing the mass and momentum transfer between the phases. Thermal properties of a single-phase and two-phase equilibrium water were calculated using CoolProp [17]. The model was written in python, and the equations were solved using the Scipy library [18].

2. EJECTOR MODEL

In this section the mathematical model of the two-phase ejector will be presented with a focus on the ejector's mixer. The model is developed by dividing the ejector into four main parts as shown in Fig. 1. The figure shows that two streams enter the ejector, the motive stream (A) is a high-pressure liquid fluid going into the motive nozzle (1). The suction stream (B) is a low-pressure gas fluid that gets entrained into the suction nozzle (2). Both streams start to interact and mix in the mixer (3) thereby exchanging mass, momentum and energy. Depending on the flow characteristics a shock wave (C) may occur downstream of the mixer. The conditions for the shock wave to occur is for the mixture flow to be supersonic. Exact representation of the characteristics of the mixture flow will be provided later in this section. Afterwards, a diffuser is used to increase the final pressure of the mixture. Figure 2 illustrates an example of the integration of an ejector within an open heat pump system. The depicted schematic demonstrates the process whereby condensate liquid water is pressurized and subsequently sent into the motive nozzle. At the same time, superheated steam is drawn into the ejector mixer. The primary function of the ejector is to increase

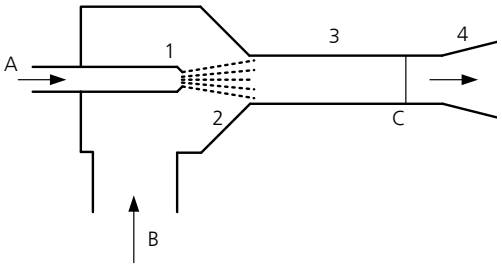

FIGURE 1: General scheme of an ejector, description in text

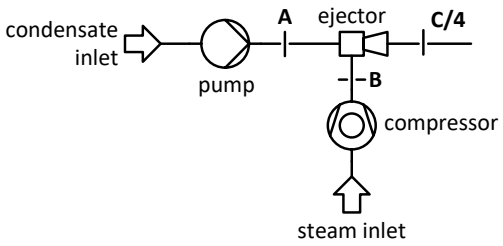

FIGURE 2: Open heat pump with an ejector as a compression step

the pressure of the resulting two-phase flow to a level more than that of the suction fluid while cooling the superheated steam coming from the compressor. This pressurized mixture is then sent to the heat sink for supplying heat. In this section, the comprehensive mathematical representation of the motive and suction nozzles is described first. This is followed by an in-depth analysis of the mixer model, explaining the methodologies employed in the computation of the mixture properties.

2.1 Mathematical Modelling of Motive and Suction Nozzles

The motive nozzle's design in an ejector varies based on its specific use. It can be convergent, where the ejector functions in a subsonic regime, potentially reaching sonic speeds at the nozzle's exit under certain conditions. Alternatively, it might be convergent-divergent, enabling the flow to achieve supersonic velocities at the nozzle's exit. The selection of nozzle type is primarily influenced by the ejector's intended application. In supersonic nozzles, the fluid crosses its saturation line during the expansion process, resulting in a metastable state and the flashing of water. This leads to the creation of a two-phase fluid flow already in the motive nozzle, making the simulation process complex. Various models, including the one done by Tammone et al. [19], have been developed for simulating water flashing in convergent-divergent nozzles. This study, however, focuses on a purely convergent nozzle for two main reasons. Firstly, the convergent nozzle may induce a spraying cone of water, which may better blend with the steam in the mixer. This becomes particularly important for future experimental work, where the nozzle choice is crucial for the ejector performance. Secondly, to avoid additional complexity in the simulation model due to the fluid's metastability and water flashing, two-phase interactions are limited only to the ejector's mixer. The metastable case modelling also needs new calibration of the respective models

for the case of water. This part of the model is reserved for a future publication in which experimental data will be available by the authors. The numerical algorithm used to design and simulate the motive and suction nozzles is as following [9]:

- First the initial static pressure p, static temperature T and mass flow rate $\dot{m}$ are given at the nozzle inlet.
- Empirical correlations provided the basis for determining the pressure at the nozzle exit. These correlations indicate that the exit pressure typically approximates 90% of the pressure observed at the inlet of the suction nozzle [16].
- A small value of pressure decrease Δp is applied assuming isentropic expansion.
- This will result in a change in static temperature ΔT and consequently specific enthalpy Δh.
- The corresponding velocity case can be calculated from the enthalpy change and the nozzle efficiency, $w = \sqrt{2\Delta h \zeta_n}$.
- The area at this cross section can then be calculated from the mass flow rate, density and the velocity at the corresponding Δp, $A = \dot{m}/\rho w$
- The process is repeated until the final pressure is equal the nozzle exit pressure.

The algorithm assumes a steady-state, single phase flow. Drag and viscous effects between the nozzle and flow is accounted by the nozzle efficiency ζ whose value is taken as 85% for both the motive and suction nozzles according to the recommendations made by Šarevski and Šarevski [9].

2.2 Mixer

Modelling of the mixer is the core work of this paper. In the mixer, the expanded water condensate at the exit of the motive nozzle is at a high velocity. The intention here is to use this high velocity and the expansion of water to entrain the superheated steam coming from the compressor. The steam will lose some of its pressure in the entrainment process but it is still at a much higher static temperature and lower velocity compared to the condensate water. Most 1D models typically assume that the two-fluids will be at the same saturation temperature in the mixer which is not the case here. Indeed, the significant divergence in temperature and velocity between the liquid water and steam within the mixer under investigation is a distinctive aspect of this research, posing unique challenges in simulating the various interactions between the two phases. To address this, the existing 1D model initially made for CO_2 ejector's by Banasiak and Hafner [13] and later further developed by Wilhelmsen et al. [12] has been adopted and modified here. Similar key assumptions as those mentioned in their work were made in the current work, though some modifications were introduced:

- Both streams entering the mixer form a coaxial double-fluid flow, where the motive stream flows in the center and the suction stream flows in the annulus. The approach was originally proposed by Narabayashi et al. [20].
- Uniform static pressure level is assumed for both streams, a common practice in both 0D and multidimensional models of mixing processes, as discussed by He et al. [21].
- The streams undergo mass, momentum, and energy exchange along their trajectory.
- Two distinctive mechanisms accounts for the mass transfer: evaporation of the motive stream and entrainment of the suction stream by the motive stream.
- Momentum transfer is characterized by interfacial drag forces between the streams, and the momentum transfer due to mass transfer.
- Energy transfer is considered through enthalpy and velocity variations resulting from mass transfer.
- Frictional pressure drop is accounted for, not only at the wall boundary layer, but also across a hypothetical, infinitesimal 'mixing layer' that separates the streams. The computational approach is similar to that employed for wall friction factor evaluation.
- The enthalpy of the combined flow is determined utilizing the mixer energy balance.

For a single phase flow, the governing conservation equations neglecting internal heat sources and gravity forces for mass, momentum and energy constitute a system of ordinary differential equations:

- Continuity equation:

$$\frac{\partial \rho}{\partial t} + \frac{\partial (\rho u)}{\partial x} = 0 \tag{1}$$

- Momentum equation:

$$\frac{\partial (\rho u)}{\partial t} + \frac{\partial (\rho u^2)}{\partial x} + \frac{\partial (p)}{\partial x} = 0 \tag{2}$$

- Energy equation:

$$\frac{\partial}{\partial t}\left(\rho e + \frac{1}{2}\rho u^2\right) + \frac{\partial}{\partial x}\left[\rho u \left(h + \frac{1}{2}u^2\right)\right] = 0 \tag{3}$$

For multiphase simulations, the above equations can be extended to simulate two-phase fluid following the pseudo fluid approach [22]. In this approach, the system of governing equation for both the motive and suction stream can be written in an array notation:

$$\boldsymbol{\Omega} \cdot \boldsymbol{X} = \boldsymbol{B} \tag{4}$$

Ω here is the coefficient matrix containing the constants by which the various flow variables are multiplied with. $\mathbf{X}$ is the state vector matrix containing the various thermodynamic properties being solved for. $\mathbf{B}$ is the source term matrix containing the source terms for mass transfer between the phases, friction force at the wall and at the interface, momentum transfer and energy

transfer. The array notation is a common form of writing the Euler equations in gas dynamic and is often adapted to multiphase flow models. The arrays **X** (5), Ω (6) and **B** (7) can be defined as follows:

$$X_{mix}^{T} = \left[\frac{dp}{dx} \quad \frac{dw_m}{dx} \quad \frac{dw_s}{dx} \quad \frac{dh_m}{dx} \quad \frac{dh_s}{dx} \quad \frac{d\rho_m}{dx} \quad \frac{d\rho_s}{dx} \quad \frac{dA_m}{dx} \quad \frac{dA_s}{dx}\right] \tag{5}$$

As previously said, matrix ***B*** contains the source terms pertinent to the mass, momentum, and energy transfer between phases. Focusing first on mass transfer, and more specifically on the differential aspect of evaporation mass transfer at the interface, it is characterized by the following expression:

$$\frac{d\Gamma_e}{dx} = \frac{\alpha_{\text{int}}(T_s - T_m)}{h_{\text{sat,v}} - h_{\text{int}}} \cdot \frac{dF_{int}}{dx} \tag{8}$$

The static temperature of the suction stream always exceeds that of the motive stream. Consequently, Eq. 8 quantifies the energy transfer from the suction to the motive stream, normalized by the energy threshold required for evaporation. The interfacial heat transfer coefficient, denoted as α_{int}, is determined using the Dittus-Boelter equation as cited in Kolev [23]. This calculation necessitates the specification of interfacial properties. Given that the emphasis here is on the evaporation of the motive fluid, the interfacial properties have been aligned with those of the motive fluid, i.e. $h_{int} = h_m$.

Mass transfer via entrainment in the suction stream is vital for the ejector's efficiency. Efficient entrainment enhances mixing and energy exchange, thereby improving the ejector's capacity to compress the mixed fluid. Eq. 9 shows the mass transfer by suction stream entrainment given by Schadel correlation that is provided by Kolev [23]:

$$\frac{d\Gamma_{s\to m}}{dx} = \begin{cases} A \cdot w_m \sqrt{\rho_m \rho_s} \cdot \eta_s \cdot (Re_s - Re_{s,\infty}) \cdot \frac{dF_{int}}{dx}, & \text{if } Re_s \geq Re_{s,\infty} \\ 0 & \text{otherwise} \end{cases} \tag{9}$$

where A = 1.175×10^{-4} m.s kg^{-1}. The local equilibrium film Reynolds number is given by:

$$Re_{s_\infty} = \exp\left(5.8504 + 0.4249\left(\frac{\eta_m}{\eta_s}\right)\sqrt{\frac{\rho_s}{\rho_m}}\right) \tag{10}$$

Two sources for friction forces are presented in matrix ***B*** (7), the friction at the interface between the two streams given by:

$$\frac{dWf,int}{dx} = 0.5 \cdot f_{\text{int}} \cdot \rho_m \cdot (w_m - w_s)^2 \cdot \frac{dF_{int}}{dx} \tag{11}$$

The other source term of friction is the friction of the suction stream with the wall given by the following relation:

$$\frac{dW_{f,w}}{dx} = 0.5 \cdot f_w \cdot \rho_s \cdot w_s^2 \cdot \frac{dF_w}{dx} \tag{12}$$

Both friction factors in Eq. 11 and Eq. 12 were determined according to the Churchill model [24]. The model, originally formulated for single-phase flow within conduits of circular cross-section, is extendable to the analysis of two-phase homogeneous flow within mini-channels. This can be done assuming an equivalent two-phase viscosity to characterize the flow [13]. Equation 13 represents the Churchill model:

$$f = 8\left(\left(\left(\frac{8}{\text{Re}}\right)^{12} + \left(\frac{1}{A+B}\right)^{1.5}\right)^{\frac{1}{12}}\right) \tag{13}$$

where:

$$A = \left(2.457 \log\left(\frac{1}{\left(\left(\frac{7}{\text{Re}}\right)^{0.9} + 0.27\left(\frac{\varepsilon}{D_h}\right)\right)}\right)\right)^{16} \tag{14}$$

$$B = \left(\frac{37530}{\text{Re}}\right)^{16} \tag{15}$$

It can be seen from Eq. 14 that a roughness factor ϵ needs to be applied at both the interface and the wall. This factor considers the hydrodynamic irregularity at the two-phase flow interface, considering the relative slip velocity between the phases. Banasiak and Hafner [13] refined these values empirically, calibrating them against experiments done on CO_2 ejectors. Meknassi et al. [25] have reported roughness factors based on empirical data for two-phase air-water flow systems. Thus, the roughness values employed herein are taken as an initial approximation, analogous to the findings reported by [25]. Another important source term present in the flow is the momentum transfer rate:

$$\frac{d\Pi}{dx} = 0.5 \cdot \rho_m \cdot C_{m\to s} \cdot |w_m - w_s| \cdot (w_m - w_s) \cdot \frac{dF_{\text{int}}}{dx} \tag{16}$$

where:

$$\text{Re}_{m\to s} = \left(\frac{\rho_s}{\eta_s}\right) \cdot (w_m - w_s) \cdot D_{\text{m}} \cdot \sqrt{\frac{A_m}{A_m + A_s}} \tag{17}$$

$$C_{m\to s} = a \cdot \text{Re}_{m\to s}^{-0.25} \tag{18}$$

The directional notation in the momentum transfer equations above emphasizes that the momentum transfer from the motive fluid to the suction fluid. This phenomenon aligns with the intended effect, as the motive stream comes with a higher velocity. Consequently, the applicability of the equation is valid on the condition that the velocity of the motive fluid is always higher that of the suction fluid. The diameter D in Eq. 17 is the inner diameter of the co-axial flow, i.e. the diameter of the motive stream. The value of the drag coefficient C in Eq. 18 is a function of the coefficient of scale (a) which is experimentally determined. Aritomi et al. [26] conducted an empirical analysis of the thermo-hydraulic characteristics of inverted annular water flow. They identified a scale coefficient (a) value of 0.3164. This coefficient has been adopted in the current simulations, due to the realtive similarity between their investigated scenario and the case under simulation in this research.

$$\Omega_{mix} = \begin{bmatrix} 0 & \frac{1}{w_m} & 0 & 0 & 0 & \frac{1}{\rho_m} & 0 & \frac{1}{A_m} & 0 \\ 0 & 0 & \frac{1}{w_s} & 0 & 0 & 0 & \frac{1}{\rho_s} & 0 & \frac{1}{A_s} \\ A_m & A_m w_m \rho_m & 0 & 0 & 0 & 0 & 0 & 0 & 0 \\ A_s & 0 & A_s w_s \rho_s & 0 & 0 & 0 & 0 & 0 & 0 \\ 0 & A_m w_m^2 \rho_m & 0 & A_m w_m \rho_m & 0 & 0 & 0 & 0 & 0 \\ 0 & 0 & A_s w_s^2 \rho_s & 0 & A_s w_s \rho_s & 0 & 0 & 0 & 0 \\ \frac{1}{c_m^2} - \frac{\frac{\partial \rho_m}{\partial s}\Big|_p}{T_m \rho_m} & 0 & 0 & \frac{\frac{\partial \rho_m}{\partial s}\Big|_p}{T_m} & 0 & -1 & 0 & 0 & 0 \\ \frac{1}{c_s^2} - \frac{\frac{\partial \rho_s}{\partial s}\Big|_p}{T_s \rho_s} & 0 & 0 & 0 & \frac{\frac{\partial \rho_s}{\partial s}\Big|_p}{T_s} & 0 & -1 & 0 & 0 \\ 0 & 0 & 0 & 0 & 0 & 0 & 0 & 1 & 1 \end{bmatrix} \tag{6}$$

$$B_{mix} = \begin{bmatrix} -\frac{1}{A_m w_m \rho_m}\left(\frac{d\Gamma_e}{dx} + \frac{d\Gamma_{s\to m}}{dx}\right) \\ \frac{1}{A_s w_s \rho_s}\left(\frac{d\Gamma_e}{dx} - \frac{d\Gamma_{s\to m}}{dx}\right) \\ -(w_{int} - w_m)\frac{d\Gamma_e}{dx} + (w_s - w_m)\frac{d\Gamma_{s\to m}}{dx} - \frac{d\Pi}{dx} - \frac{dW_{f,int}}{dx} \\ -(w_s - w_{int})\frac{d\Gamma_e}{dx} + \frac{d\Pi}{dx} - \frac{dW_{f,w}}{dx} \\ (h_m - h_{int} + \frac{1}{2}(w_m^2 - w_{int}^2))\frac{d\Gamma_e}{dx} + (h_s - h_m + \frac{1}{2}(w_s^2 - w_m^2))\frac{d\Gamma_{s\to m}}{dx} \\ (h_{int} - h_s + \frac{1}{2}(w_{int}^2 - w_s^2))\frac{d\Gamma_e}{dx} \\ 0 \\ 0 \\ \frac{dA_{total}}{dx} \end{bmatrix} \tag{7}$$

2.3 Two-Phase Speed of Sound Modelling

Depending on the flow conditions, a shock wave can occur downstream of the mixer. The condition for this shock to occur is when the mixture velocity is higher than the speed of sound velocity for the two-phase mixture, i.e. when the Mach number of the mixed flow is higher than 1. The velocity of the mixed flow is calculated as following:

$$w_{\text{mix}} = w_m m_m + w_s m_s \tag{19}$$

where:

$$m_m = \frac{\dot{m}_m}{\dot{m}_m + \dot{m}_s} \tag{20}$$

$$m_s = \frac{\dot{m}_s}{\dot{m}_m + \dot{m}_s} \tag{21}$$

For the speed of sound, the CoolProp formulation is only valid for homogeneous (single-phase) state. The two-phase properties are not defined and for many fluids are invalid [17]. That is why several models have been proposed to compute the speed of sound for two-phase mixture. The homogeneous equilibrium model is a well-known and commonly used model for two-phase flow simulations [27]. The model proposed the following relation for the speed of sound:

$$c_{\text{HEM}}^2 = -v_{mix}^2 \left\{ \left(\frac{dv_l}{dp}\right) - \left(\frac{ds}{dp}\right)_x \frac{v_v - v_l}{s_v - s_l} + x\left[\left(\frac{v_v}{dp}\right) - \left(\frac{dv_l}{dp}\right)\right] \right\}^{-1} \tag{22}$$

where:

$$v_{mix} = \rho_{mix}^{-1} = \beta \cdot \rho_v + (1 - \beta) \cdot \rho_l \tag{23}$$

and:

$$\beta_h = \left[1 + \left(\frac{1-x}{x}\right)\left(\frac{\rho_g}{\rho_l}\right)\right]^{-1} \tag{24}$$

The void fraction β defined in Eq. 24 is a homogeneous correlation derived by treating the vapor and liquid phases as a homogeneous mixture [28]. The Mach number M of the mixed flow within the ejector is determined by employing the velocity of the mixed flow, Eq. 19, in conjunction with the two-phase speed of sound, Eq. 22. A Mach number more than unity indicates a potential occurrence of a shock wave within the mixer. This phenomenon is critical for the analysis of flow within the ejector, as the presence of a shock wave significantly influences the overall ejector performance.

2.4 Shock Wave Modelling

The relationships between various flow variables across the terminal states of a normal shock in an ideal gas are describable as functions of the upstream Mach number. These relationships are commonly known as the Rankine-Hugoniot relations [22]. However, extending these relations to scenarios involving shock waves in vapor-droplet mixtures presents considerable complexity. This complexity primarily stems from the mass transfer inherent in two-phase systems. Guha [29] has derived analytical jump conditions across normal shock waves in wet steams flow. These equations were used here to determine the pressure rise and the flow conditions downstream of a shock wave in case of its occurrence in the mixer section of the ejector:

$$\frac{p_{as}}{p_{bs}} = \left(\frac{2 \cdot \kappa}{\kappa + 1} \cdot M_{bs}^2 - \frac{\kappa - 1}{\kappa + 1}\right) \tag{25}$$

$$\frac{w_{\text{mix, as}}}{w_{\text{mix, bs}}} = \frac{(\kappa_{\text{bs}} - 1) \cdot \text{M}_{\text{bs}}^2 + 2}{(\kappa_{\text{bs}} + 1) \cdot \text{M}_{\text{bs}}^2} \tag{26}$$

$$\frac{\rho_{\text{mix, as}}}{\rho_{\text{mix, bs}}} = \frac{w_{\text{mix, bs}}}{w_{\text{mix, as}}} \tag{27}$$

where κ is the isentropic expansion coefficient defined by Eq. 28 and is state-specific property for non-ideal fluids [30]:

$$\kappa = -\left(\frac{v}{p}\right)\left(\frac{\partial p}{\partial v}\right)_{\text{s}} \tag{28}$$

and M_{bs} is the Mach number before the shock wave defined as:

$$\text{M}_{\text{bs}} = \frac{w_{\text{mix}}}{c_{\text{HEM}}} \tag{29}$$

The aforementioned equations have been used to determine the properties of the mixture flow subsequent to the potential occurrence of a shock wave and prior to the flow into the diffuser. This analysis is important for understanding the flow characteristics induced by the shock wave, thereby providing a more precise evaluation of the flow behavior in the diffuser.

2.5 Diffuser Modelling

The diffuser is the final part of the ejector, it comes after the mixer with the intended use to add an additional increment of pressure to the flow. In case the occurrence of a shock wave downstream of the mixer, and if the shock wave is strong enough, the liquid droplets will get dispersed in the steam phase. The resulting flow will then be a mist flow which can be modelled in a similar way to the mixer:

$$\Omega_{diff} = \begin{bmatrix} 0 & \frac{1}{w} & 0 & \frac{1}{\rho} \\ A & Aw\rho & 0 & 0 \\ 0 & w & 1 & 0 \\ \left(\frac{\partial \rho}{\partial p} - \frac{1}{T\rho}\frac{\partial \rho}{\partial S}\right) & 0 & \frac{1}{T}\frac{\partial \rho}{\partial S} & -1 \end{bmatrix} \tag{30}$$

The B matrix (source term matrix) is given by:

$$B_{diff} = \begin{bmatrix} -\frac{1}{A}\frac{\partial A}{\partial x} \\ -f\rho\frac{w^2}{2}\frac{\partial F}{\partial x} \\ 0 \\ 0 \end{bmatrix} \tag{31}$$

$$X_{diff}^T = \begin{bmatrix} \frac{dp}{dx} & \frac{dw}{dx} & \frac{dh}{dx} & \frac{rho}{dx} \end{bmatrix} \tag{32}$$

The equation for the derivative of density with respect to pressure is given by:

$$\frac{\partial \rho}{\partial p} = \left(\frac{\bar{\rho}}{\rho_{l,sat}}\right)^2 \cdot (1 - \beta) \cdot \frac{\partial \rho_{l,\text{sat}}}{\partial p} + \left(\frac{\bar{\rho}}{\rho_{v,sat}}\right)^2 \cdot \beta \cdot \frac{\partial \rho_{v,\text{sat}}}{\partial p} \tag{33}$$

where $\bar{\rho}$ is:

$$\bar{\rho} = \beta \cdot \rho_v + (1 - \beta) \cdot \rho_l \tag{34}$$

and $\frac{\partial \rho}{\partial s}$ was calculated in a similar way as to Eq. 33.

The boundary conditions of the simulations were the inlet pressures, specific enthalpies and mass flow rates for both the motive and the suction stream. These values were based on a preliminary 0D study performed by the authors that considered modelling of this ejector for a high-temperature steam heat pump application [16]. The system of Eqs. was written and solved in python using Scipy [18] as a solver for the ordinary differential equations implementing the Runge-Kutta method of order 4(5), which means it is a fourth-order method with an option to estimate the error and adjust the step size to achieve a fifth-order accuracy.

TABLE 1: Model's inlet conditions

Variable	Value
Motive nozzle inlet pressure	120 bar
Suction nozzle inlet pressure	1.7 bar
Motive nozzle inlet temperature	363 K
Suction nozzle inlet temperature	444 K
Motive fluid mass flow rate	2 kg/s
Suction fluid mass flow rate	0.2 kg/s
Suction fluid degree of superheat	55 K
Entrainment ratio	0.1

3. RESULTS AND DISCUSSIONS

3.1 Local Variable Profiles in the Reference Case

This modelling effort focuses on the mixer, aiming to outline local profiles of key flow variables such as pressure (p), velocity (w), and Mach number (M). These profiles are tailored to a specific set of inlet conditions, as detailed in Table 1. The rationale behind selecting these particular inlet variable values stems from prior 0D modelling conducted on this ejector, as reported in a preceding study [16]. This scenario will henceforth be referred to as the 'reference case', serving as a benchmark for subsequent analyses involving variations in these variables. The local profile corresponding to the reference case is depicted in Fig. 3. In the pressure profiles depicted in Fig. 3, observing variations in the suction flow and mixer pressures presents a challenge, primarily due to the significantly higher motive fluid inlet pressure of 120 bar, compared to the suction fluid and mixer pressures, which lie within the 1.5 - 2 bar range. For this reason, a detailed analyses of the pressure change in the mixer will be give in section 3.2. A noteworthy aspect of the overall figure is the apparent discontinuity in the motive fluid curves. This discontinuity arises due to the motive nozzle's shorter length relative to the suction nozzle, with the mixer starting at the end of the suction nozzle. Going more in details in Fig. 3 we can notice the following:

- In the motive and suction nozzles, the pressure, velocity and temperature of the both fluids have changed as expected with the velocity increasing and pressure and temperature decreasing.
- Upon entering the mixer, the two fluids start mixing, the motive fluid drags and increase the velocity of the suction fluid. At the same time, the temperature of the motive fluid decreases. The reason for this could be that the motive fluid is moving within the core of the mixer while being surrounded by the suction fluid of a much higher temperature. Therefore, the motive fluid starts evaporating while taking the heat

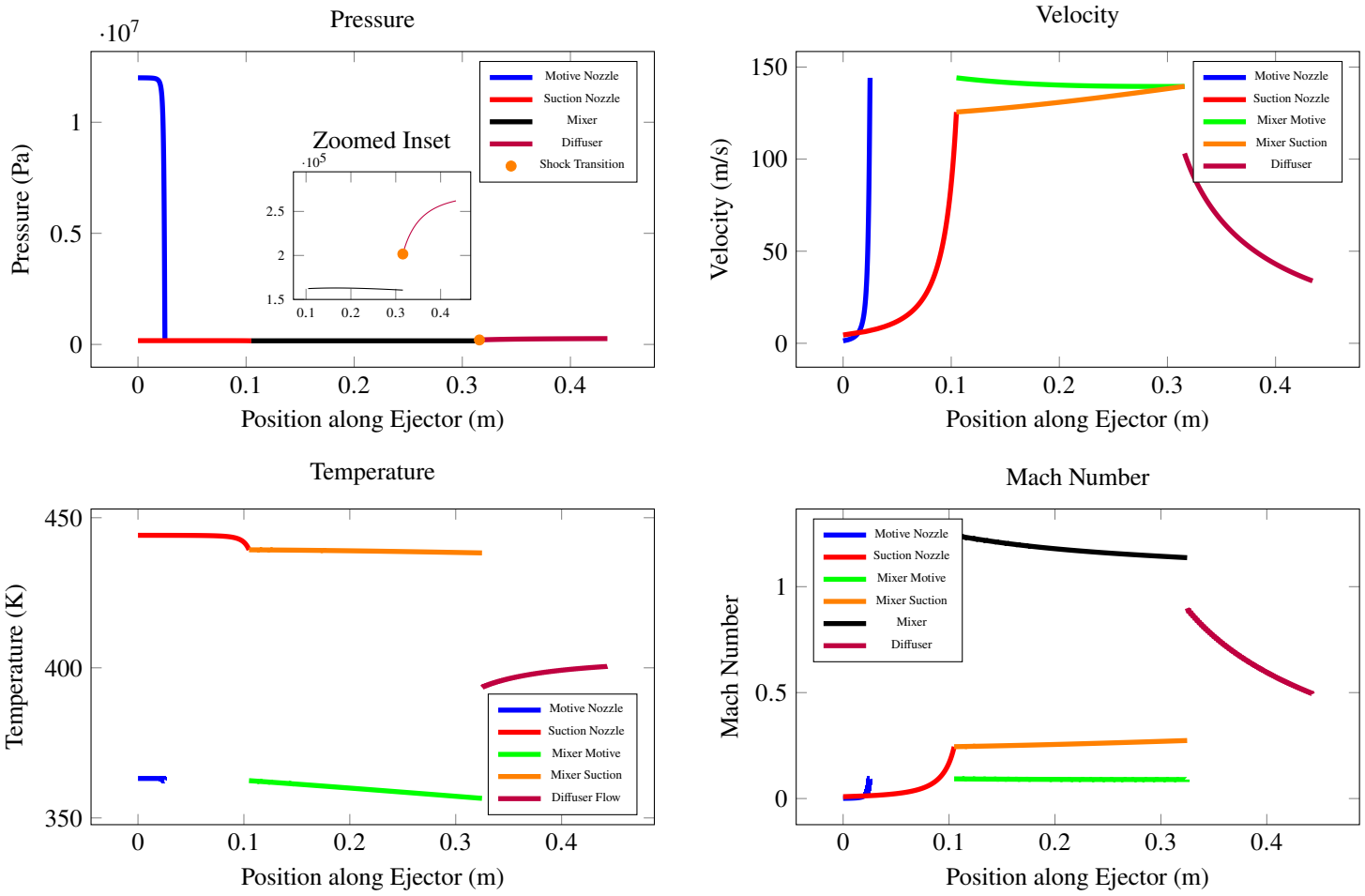

FIGURE 3: Ejector Profiles: Pressure, Velocity, Temperature, and Mach Number for the Reference Case presented in Table 1

from its core temperature, thereby causing a reduction in its temperature.

- From the pressure profile it can be seen that a shock has occurred at the end of the mixer causing by that an increase in pressure (shown as an orange dot in the pressure profile). Though a closer look at the Mach number plots in Fig. 3 shows that the Mach numbers for both the motive and suction fluids are subsonic (below 1). In fact in the Mach number plot there are three lines in the mixer section, one for the mixer motive (shown in green) and mixer suction (shown in orange) and one for the combined Mach number for the mixer flow (shown in black). Here a crucial point must be highlighted that the combined Mach number of the motive and suction fluids in the mixer is computed based on the HEM discussed in subsection 2.3. This implies that the two-phase mixture exhibits a distinct density and, consequently, a different speed of sound, typically much lower than that of a single-phase flow. Furthermore, the occurrence of a shock is assumed at the position where the velocities of the motive and suction fluids equalize, shown at the end of the mixer. This is a critical point where it is assumed that mechanical equilibrium is attained and the two fluids have merged.

- The pressure increase across the shock wave was determined in accordance with the equations presented in subsection 2.4. The flow properties prior to and subsequent to the shock wave, for the reference case, are presented in Table 2.

- As can be seen from Table 2, the Mach number of the mixture before the shock is above 1 creating thereby a shock wave and increasing the pressure of the flow by a factor of almost 1.25.

- The shock wave is assumed to occur at the end of the mixer where afterwards the flow is simulated as a two-phase homogeneous flow in the diffuser.

- After the shock, the mixture pressure continue to increase in the diffuser reaching a final pressure of around 2.6 bar as shown in the zoomed inset in the pressure plot in Fig. 3.

- It can be seen from Table 2 that part of the flow has been condensed due to the strong nature of the shock resulting in a decrease of the mass vapor content in the flow. Such a decrease in quality has been reported in previous literature in two-phase flow in ejectors [14, 15].

- In the diffuser the pressure, velocity and temperature of the

TABLE 2: Flow Properties Before and After the Shock Wave

Property	Before Shock	After Shock
Velocity (m/s)	140	104
Pressure (bar)	1.60	2.00
Temperature (K)	386	393
Quality	0.113	0.103
Mach Number	1.137	0.879

mixture has changed as expected with the velocity decreasing and pressure and temperature increasing.

The results presented in Fig. 3 and Table 2 underscore the considerable potential of ejectors in enhancing pressure and temperature parameters. However, it is crucial to support these findings through empirical validation and experimental testing.

3.2 Mixer Local Variables Profiles

Figure 4 illustrates the pressure and velocity profiles within the mixer for the reference case. An analysis of this figure reveals a marginal decrease in pressure, approximately 0.025 bar, across the mixer. This phenomenon is mostly due to the mechanical non-equilibrium within the co-axial flow, as characterized by the drag coefficient presented in Eq. 18. At the same time, the velocity profiles of the flows in both the motive and suction nozzles align with anticipated behavior. The motive fluid, entering at a higher velocity, engages in a vigorous momentum exchange with the suction fluid. Owing to the lower density of the suction fluid, it experiences an acceleration. This momentum exchange persists until the point of velocity equilibrium is achieved between the two fluids. It might be assumed that the velocity profiles of the two phases would exhibit mirror symmetry, implying congruent but inversely oriented shapes. This assumption could hold in scenarios where only momentum exchange occurs between the phases. However, in the context of this study, such a simplification does not accurately represent the dynamics in question. Referring back to the source terms matrix (B) outlined in 7, it becomes evident that additional source terms significantly influence the velocity profiles of both streams. For instance, in the case of the suction fluid, an additional frictional force exerted by the wall contributes to the modification of its velocity profile. Conversely, the entrainment of the suction flow into the motive flow impacts the reduction pattern of the motive fluid's velocity. This phenomenon, where the velocity profiles of the motive and suction fluids within the ejector mixer assume distinct shapes, has been similarly shown in the study by Wilhelmsen et al. [12].

3.3 Parameter Study on Mixers Variable Local Profiles

The inlet parameters for the suction nozzle are predominantly determined by the design specifications of the compressor and the heat pump. However, a scope for optimization still exist in the selection of inlet variables for the motive stream, particularly concerning the inlet pressures, temperatures, and mass flow rates. The subsequent subsections will investigate the impact of variations in these three variables on the local pressure and velocity profiles of both the motive and suction steams within the mixer.

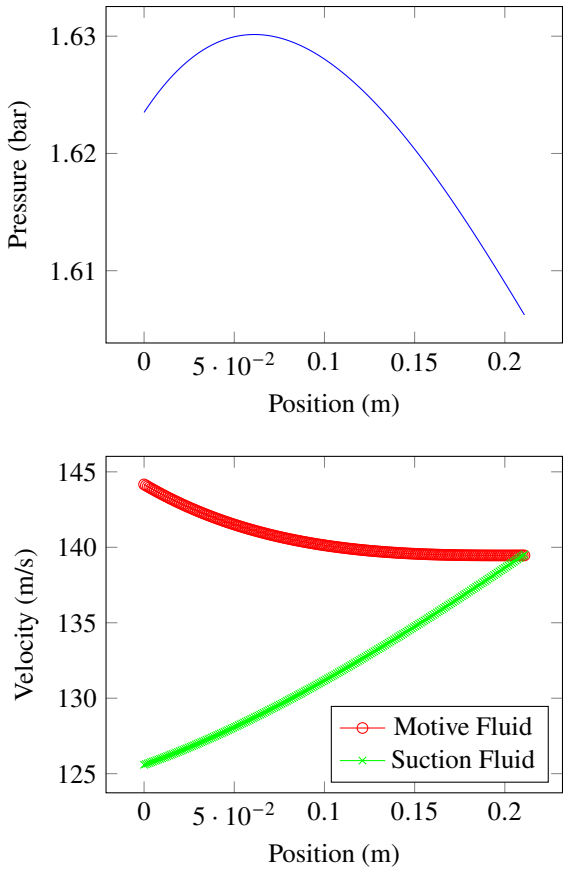

FIGURE 4: Pressure and Velocity Profiles in the Mixer, Reference Case, x = 0 at the Mixer Inlet

Changing the Motive Fluid Inlet Pressure. The inlet pressure of the motive nozzle was varied from 120 bar to 160 bar, and the corresponding effects on mixer pressure and velocity profiles for both the motive and suction fluids are depicted in Fig. 5. The figure shows that an increase in the motive nozzle inlet pressure increases the difference in velocities between the motive and suction flows. This requires an extended mixer length to allow sufficient length for the flows to attain the same velocity, thereby reaching mechanical equilibrium. Additionally, it is observed that the reduction in pressure within the mixer is less pronounced at higher inlet pressures of the motive fluid. This may be attributed to the increased energy content in the flow at elevated pressures, resulting in a lower pressure drop due to frictional interactions between the interface and the wall and even a higher mixer pressure. It is also noteworthy that at motive fluid inlet pressures below 110 bar, the velocity difference between the motive and suction flows diminishes significantly, to the extent that the ejector's functionality is compromised.

Changing the Motive Fluid Inlet Temperature. Figure 6 shows the impact of varying the inlet temperature of the motive fluid at the motive nozzle inlet. Analysis of the figure reveals that changing the inlet temperature have a marginal effect on the pressure and velocity profiles of the two fluid streams. A reduction in the inlet temperature is observed to slightly decrease the pressure within the mixer, alongside a slight reduction in the

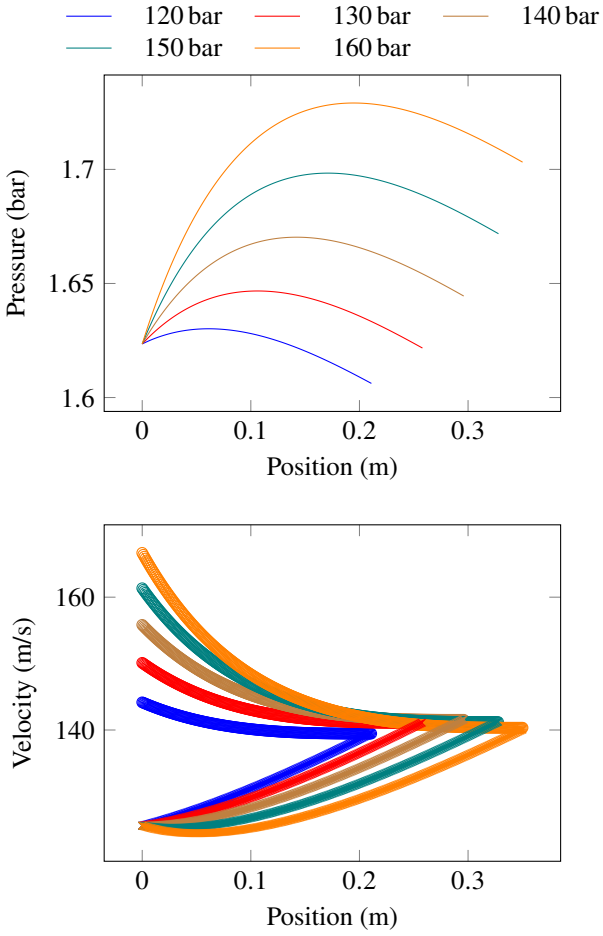

FIGURE 5: Pressure and Velocity Profiles in the Mixer (circles: motive fluid, crosses: suction fluid), p_{mn} varied from 120 bar **to** 160 bar**.**

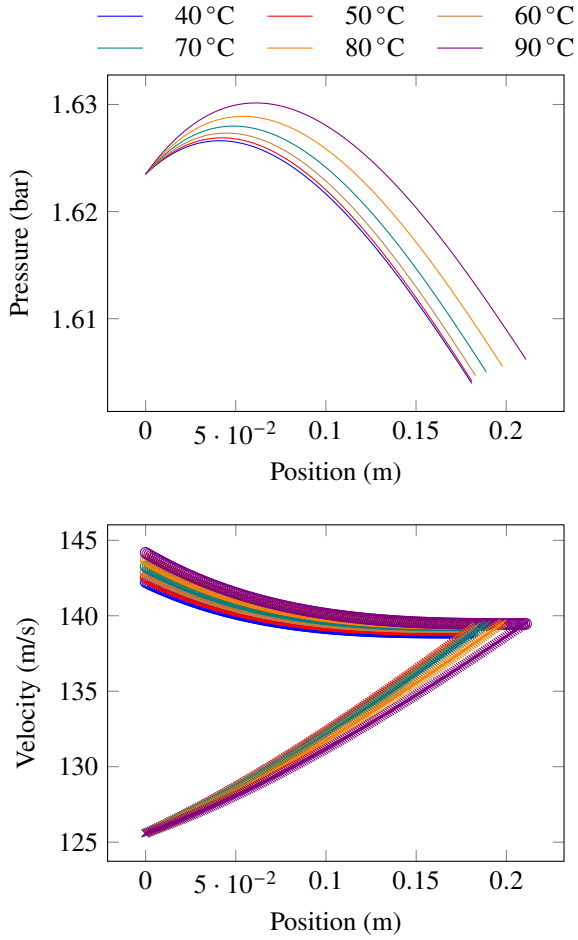

FIGURE 6: Pressure and Velocity Profiles in the Mixer (circles: motive fluid, crosses: suction fluid), Inlet Temperature varied from 40 °C **to** 90 °C**.**

velocity of the stream. This can be attributed to the reduced energy content coming with lower inlet temperatures.

Changing the Motive Fluid Inlet Mass Flow Rate.

The entrainment ratio, defined as the ratio of suction to motive fluid mass flow, exerts a significant influence on ejector performance. In the reference case, this ratio was given as 0.1 (see Table 1), aligning with the entrainment ratios provided in the literature for two-phase ejectors, which range from 0.1 to 0.6 [9, 13]. Ejectors are designed to achieve optimal performance at a specific design point and therefore, they do not preform optimally in off-design conditions [4, 9]. In the simulation presented here, variations in the entrainment ratio were observed to significantly impact the ejector functionality. Specifically, increasing the entrainment ratio have resulted in an inadequate water flow, thereby hindering sufficient entrainment of the suction flow. Conversely, lowering the entrainment ratio led to an excessive water content, thereby resulting in a complete condensation within the ejector system. These findings highlights the necessity for further research aimed at defining the ejector geometry to align with the range of potential inlet conditions and the desired output.

4. CONCLUSION

In this study, the application of a one-dimensional (1D) model for simulating two-phase water steam ejectors in high-temperature heat pump applications is adopted and refined. Operating on the principles of a pseudo-fluid approach, the model integrates mechanical and thermal non-equilibrium between water and steam phases through various source terms accounting for mass, momentum, and energy exchanges. This approach has been crucial in identifying critical minimum threshold values, under which the functionality of the ejector is restricted, particularly under constant suction fluid input conditions. The formation of a shock wave at the mixer's end, where motive and suction fluids merge and reach mechanical equilibrium, has been observed to increase the pressure and temperature of the mixture flow. This pressure increase has been further augmented by the diffuser. The total pressure ratio of the ejector was about 1.5 based on the studied references case. This finding highlights the potential of two-phase water steam ejectors as potential steam compressors. Empirical validation of these findings is planned in future research by the authors, which is crucial for reinforcing the theoretical model. Additionally, this research highlight the necessity of evaluating and optimizing the ejector's performance

relative to the specific cycle of deployment, with a specific focus on achieving the desired parameters at the ejector's outlet.

REFERENCES

[1] Arpagaus, Cordin, Bless, Frédéric, Uhlmann, Michael, Schiffmann, Jürg and Bertsch, Stefan S. "High temperature heat pumps: Market overview, state of the art, research status, refrigerants, and application potentials." *Energy* Vol. 152 (2018): pp. 985–1010. DOI https://doi.org/10.1016/j.energy.2018.03.166.

[2] Kriese, Maximilian, Klöppel, Steffen, Setzepfand, Nico, Schaffrath, Robert and Nicke, Eberhard. "Part-Load Behavior and Start Up Procedure of a Reverse Rankine High Temperature Heat Pump With Water As its Working Medium." *Turbo Expo: Power for Land, Sea, and Air*, Vol. 86984: p. V005T06A027. 2023. American Society of Mechanical Engineers. DOI https://doi.org/10.1115/GT2023-103410.

[3] Zühlsdorf, Benjamin, Schlemminger, Christian, Bantle, Michael, Evenmo, Kjetil and Elmegaard, Brian. "Design recommendations for R-718 heat pumps in high temperature applications." *Proceedings of the 13th IIR Gustav Lorentzen Conference, Valencia, 2018*. 2018. IIR. DOI 10.18462/iir.gl.2018.1367.

[4] Besagni, Giorgio, Mereu, Riccardo and Inzoli, Fabio. "Ejector refrigeration: A comprehensive review." *Renewable and Sustainable Energy Reviews* Vol. 53 (2016): pp. 373–407. DOI https://doi.org/10.1016/j.rser.2015.08.059.

[5] Grazzini, Giuseppe, Milazzo, Adriano and Mazzelli, Federico. *Ejectors for efficient refrigeration: Design, applications and computational fluid dynamics*. Springer (2018). DOI https://doi.org/10.1007/978-3-319-75244-0.

[6] Elbel, Stefan and Hrnjak, Predrag. "Ejector refrigeration: an overview of historical and present developments with an emphasis on air-conditioning applications." *International Refrigeration and Air Conditioning Conference. Paper 884.* (2008)URL http://docs.lib.purdue.edu/iracc/884.

[7] Šarevski, V.N. and Šarevski, M.N. "Energy efficiency of the thermocompression refrigerating and heat pump systems." *International Journal of Refrigeration* Vol. 35 No. 4 (2012): pp. 1067–1079. DOI https://doi.org/10.1016/j.ijrefrig.2011.12.002.

[8] Šarevski, Milan N. and Šarevski, Vasko N. "Preliminary study of a novel R718 refrigeration cycle with single stage centrifugal compressor and two-phase ejector." *International Journal of Refrigeration* Vol. 40 (2014): pp. 435–449. DOI https://doi.org/10.1016/j.ijrefrig.2013.12.005.

[9] Šarevski, Milan N and Šarevski, Vasko N. "Water (R718) turbo compressor and ejector refrigeration/heat pump technology." (2016)DOI https://doi.org/10.1016/C2015-0-01782-8.

[10] Munday, John T and Bagster, David F. "A new ejector theory applied to steam jet refrigeration." *Industrial & Engineering Chemistry Process Design and Development* Vol. 16 No. 4 (1977): pp. 442–449. DOI https://doi.org/10.1021/i260064a003.

[11] Huang, B.J., Chang, J.M., Wang, C.P. and Petrenko, V.A. "A 1-D analysis of ejector performance." *International Journal of Refrigeration* Vol. 22 No. 5 (1999): pp. 354–364. DOI https://doi.org/10.1016/S0140-7007(99)00004-3.

[12] Øivind Wilhelmsen, Aasen, Ailo, Banasiak, Krzysztof, Herlyng, Halvor and Hafner, Armin. "One-dimensional mathematical modeling of two-phase ejectors: Extension to mixtures and mapping of the local exergy destruction." *Applied Thermal Engineering* Vol. 217 (2022): p. 119228. DOI https://doi.org/10.1016/j.applthermaleng.2022.119228.

[13] Banasiak, Krzysztof and Hafner, Armin. "1D Computational model of a two-phase R744 ejector for expansion work recovery." *International Journal of Thermal Sciences* Vol. 50 No. 11 (2011): pp. 2235–2247. DOI https://doi.org/10.1016/j.ijthermalsci.2011.06.007.

[14] Bergander, Mark J. "Refrigeration cycle with two-phase condensing ejector." *International Refrigeration and Air Conditioning Conference. Paper 748* (2006)URL http://docs.lib.purdue.edu/iracc/748.

[15] Alam, Md Muntasir and Elbel, Stefan. "Utilization of Ejector for Decrease of Compressor Discharge Pressure in HVAC&R Applications." *International Refrigeration and Air Conditioning Conference.Paper 2365.* (2022)URL https://docs.lib.purdue.edu/iracc/2365.

[16] Abu Khass, Omar, Tran, Anh Phong, Klöppel, Steffen and Stathopoulos, Panagiotis. "Modelling of Two-Phase Water Ejector in Rankine Cycle High Temperature Heat Pumps." *Turbo Expo: Power for Land, Sea, and Air*, Vol. 86984: p. V005T06A003. 2023. American Society of Mechanical Engineers. DOI https://doi.org/10.1115/GT2023-101245.

[17] Bell, Ian H, Wronski, Jorrit, Quoilin, Sylvain and Lemort, Vincent. "Pure and pseudo-pure fluid thermophysical property evaluation and the open-source thermophysical property library CoolProp." *Industrial & engineering chemistry research* Vol. 53 No. 6 (2014): pp. 2498–2508.

[18] Virtanen, Pauli, Gommers, Ralf, Oliphant, Travis E, Haberland, Matt, Reddy, Tyler, Cournapeau, David, Burovski, Evgeni, Peterson, Pearu, Weckesser, Warren, Bright, Jonathan et al. "SciPy 1.0: fundamental algorithms for scientific computing in Python." *Nature methods* Vol. 17 No. 3 (2020): pp. 261–272.

[19] Tammone, Carlotta, Romei, Alessandro, Persico, Giacomo and Haglind, Fredrik. "Extension of the delayed equilibrium model to flashing flows of organic fluids in converging-diverging nozzles." *International Journal of Multiphase Flow* Vol. 171 (2024): p. 104661. DOI https://doi.org/10.1016/j.ijmultiphaseflow.2023.104661.

[20] Narabayashi, Tadashi, Mizumachi, Wataru and Mori, Michitugu. "Study on two-phase flow dynamics in steam injectors." *Nuclear Engineering and Design* Vol. 175 No. 1 (1997): pp. 147–156. DOI https://doi.org/10.1016/S0029-5493(97)00170-2.

[21] He, S., Li, Y. and Wang, R.Z. "Progress of mathematical modeling on ejectors." *Renewable and Sustainable Energy Reviews* Vol. 13 No. 8 (2009): pp. 1760–1780. DOI https://doi.org/10.1016/j.rser.2008.09.032.

[22] Städtke, Herbert. *Gasdynamic aspects of two-phase flow: Hyperbolicity, wave propagation phenomena and related*

numerical methods. John Wiley & Sons (2006). DOI 10.1002/9783527610242.

[23] Kolev, Nikolay Ivanov and Kolev, NI. *Multiphase flow dynamics*. Vol. 1003. Springer (2005).

[24] Churchill, Stuart W. "Friction-factor equation spans all fluid-flow regimes." *CHEM. ENGNG; U.S.A.; DA. 1977; VOL. 84; NO 24; PP. 91-92; BIBL. 5 REF.* (1977).

[25] Meknassi, Fouad, Benkirane, Rachid, Liné, Alain and Masbernat, Lucien. "Numerical modeling of wavy stratified two-phase flow in pipes." *Chemical Engineering Science* Vol. 55 No. 20 (2000): pp. 4681–4697. DOI https://doi.org/10.1016/S0009-2509(00)00070-1.

[26] "Thermo-hydraulic behavior of inverted annular flow." *Nuclear Engineering and Design* Vol. 120 No. 2 (1990): pp. 281–291. DOI https://doi.org/10.1016/0029-5493(90)90380-G.

[27] De Lorenzo, M., Lafon, Ph., Seynhaeve, J.-M. and Bartosiewicz, Y. "Benchmark of Delayed Equilibrium Model (DEM) and classic two-phase critical flow models against experimental data." *International Journal of Multiphase Flow* Vol. 92 (2017): pp. 112–130. DOI https://doi.org/10.1016/j.ijmultiphaseflow.2017.03.004.

[28] Xu, Yu and Fang, Xiande. "Correlations of void fraction for two-phase refrigerant flow in pipes." *Applied Thermal Engineering* Vol. 64 No. 1 (2014): pp. 242–251. DOI https://doi.org/10.1016/j.applthermaleng.2013.12.032.

[29] Guha, A. "Jump conditions across normal shock waves in pure vapour–droplet flows." *Journal of Fluid Mechanics* Vol. 241 (1992): p. 349–369. DOI 10.1017/S0022112092002076.

[30] Lemmon, Eric W, Huber, Marcia L, McLinden, Mark O et al. "NIST standard reference database 23." *Reference fluid thermodynamic and transport properties (REFPROP), version* Vol. 9 (2010).